

LC Resonant Clock Resource Minimization using Compensation Capacitance

Ping-Yao Lin, Hany Ahmed Fahmy, Riadul Islam, Matthew R. Guthaus
 Department of Computer Engineering, University of California, Santa Cruz
 {plin11, hfahmy, rislam, mrg}@ucsc.edu

Abstract—Distributed-LC resonant clock distribution is a viable technique to reduce clock distribution network (CDN) dynamic power. However, resonant clocks can require significant on-chip resources to form the inductors and decoupling capacitors which discourages adoption. This paper uses a compensation capacitor (C_c) to reduce the overhead of the on-chip inductor and capacitor resources without changing the performance of a distributed-LC resonant clock. Analysis on the ISPD clock benchmarks show nearly 12% reduction in passive device area compared to previous resonant clocks while still saving 49.9% power over traditional buffered clocks.

I. INTRODUCTION

The clock distribution network (CDN) can consume 30-70% of the entire chip power due to the high switching rate and large capacitance. One way of decreasing this dynamic power is implementing resonant clocking [1]. Distributed-LC resonant clocking circumvents this dynamic power barrier by oscillating energy between an electrical potential and magnetic field in a parallel capacitance (C_{clk}) and inductance (L), respectively. An additional decoupling capacitance (C_d), serving as AC ground, offsets the voltage range to $0 - V_{dd}$ by forming a series LC tank as shown in Figure 1(a).

Industry has demonstrated power savings of these parallel LC-tank clocks [2] and confirms stable phases and magnitudes compared to standing wave [3] and rotary/salphasic [4] resonant clocks. Academic algorithms have further optimized these resonant clocks [5] and have shown to save up to 90% of the dynamic power at the expense of large inductor and decoupling capacitor on-chip area [6]. The inductor area is perhaps the most significant obstacle for significant power savings [5], [6]. In addition, the decoupling capacitance is an extra cost that is often neglected. This paper proposes a modified LC-tank topology that uses a compensation capacitor (C_c) to decrease the total inductor and capacitor area while still maintaining resonant power savings. Specifically, this paper is the first to:

- Minimize inductor and capacitor overhead in LC resonant clocks using a coupling capacitor.
- Derive the theoretical formulations how C_c and C_d affect resonant frequency.
- Provide an approximate analysis using the Miller model of C_c on resonant frequency.

The remainder of this paper proceeds as follows: Section II presents necessary background on on-chip inductance/capacitance and resonant theory. Section III introduces the theoretical formulation behind coupling capacitance in resonant clocks.

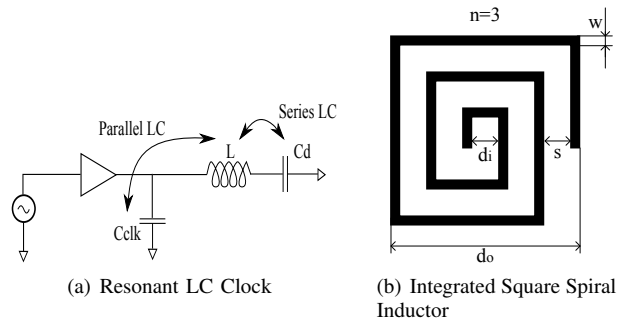


Fig. 1. Using on-chip inductors, a parallel LC_{clk} and series LC_d tank provides energy savings and voltage offset, respectively, for a resonant clock.

Section IV presents our experimental results on representative monolithic LC-tank resonant clocks and distributed LC tanks. Section V concludes the paper.

II. BACKGROUND

A. Integrated Inductors

On-chip spiral inductors can be easily manufactured in standard CMOS processes. Also, high-Q spiral inductors are available with modern processes that have thick ($\sim 10\mu m$) oxides [7]. However, on-chip inductors come with parasitic resistance and capacitance that decrease their quality factor. The parasitic resistance can be included in the model of the inductor, and the parasitic capacitance can be treated as part of the decoupling capacitance in a resonant clock [5]. The inductance of a square spiral inductor, as shown in Figure 1(b), can be approximated as

$$L = 0.002l \left[\ln \frac{2l}{w+t} + 0.5 + \frac{w+t}{3l} \right], \quad (1)$$

where l is the length of trace, w is the width of trace, and t is the thickness of the metal [8]. Given the physical parameters, the area of the inductor is

$$Area = d_o^2 = (d_i + 2n(s+w))^2, \quad (2)$$

where d_o is the outer diameter, d_i is the inner diameter, n is the number of turns, and s is the space between turns [8].

B. Integrated Capacitors

Multiple types of on-chip capacitors are utilized in ICs, such as MOS (metal-oxide-semiconductor), PIP (polysilicon-insulator-polysilicon), MIM (metal-insulator-metal), and lateral flux capacitors. These capacitors have different design and

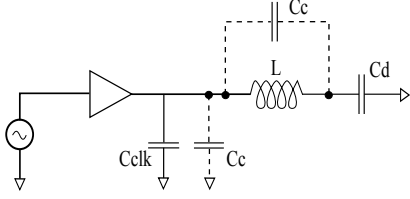


Fig. 2. Possible C_c positions to adjust resonant frequency in resonant clocks.

performance characteristics. Historically, MIM capacitors have been used in RF and mixed-signal ICs due to low leakage, high linearity, low process variations, and low temperature variations. MIM capacitors with a capacitance density comparable to MOS capacitors have been achieved by reducing the dielectric thickness and employing high-k dielectrics.

The benefit of MOS capacitors is the compatibility with CMOS technology and a high capacitance density. However, MOS capacitors exhibit challenges due to non-linearity, strong voltage dependence, and high leakage. Overall, the capacitive density of $10\text{--}20\text{ fF}/\mu\text{m}^2$ can be fabricated in modern CMOS technologies [9]. Much like inductors, the parasitic resistance in capacitors influences the efficiency of a decoupling capacitor.

C. Resonant Theory

These on-chip inductors and capacitors can be used to form a series or parallel LC “tank” circuit which resonates at a particular frequency. This so-called resonant frequency of an ideal LC tank is the frequency when the network has zero total reactance,

$$f_0 = \frac{1}{2\pi\sqrt{LC}}, \quad (3)$$

where L is the inductance and C is either the C_{clk} or C_d in our case. When the impedance of an LC tank is near infinite due to the reactances cancelling, the drive capability requirement of the clock buffer is minimized and clock energy can be saved.

As shown in Figure 1(a), our resonant clock topology contains two LC tanks: one parallel and one series. The parallel LC tank will provide infinite impedance at resonance while the series impedance will provide zero impedance. These can counteract each other if they resonate at the same frequency. Therefore, C_d is typically much larger than C_{clk} to separate the resonant frequencies of the parallel LC_{clk} and extra series LC_d tanks according to

$$\frac{1}{2\pi\sqrt{LC_d}} \ll \frac{1}{2\pi\sqrt{LC_{clk}}}. \quad (4)$$

This ensures a wide margin such as $f_{clk}/f_d \sim 3$ by making C_d usually $10 \times C_{clk}$ or more.

III. COMPENSATION CAPACITANCE

As illustrated in Figure 2, compensation capacitance (C_c) could be used in two possible topologies: one position is in parallel with C_{clk} while the second is in parallel with L . If C_c is in parallel with C_{clk} , the size of inductance can be reduced by adding to the capacitance in Equation (3) while retaining the same resonant frequency (f_0). On the other hand, if C_c is chosen in parallel with L , the Miller Effect [10]

suggests that C_c can be divided as C_{c1} and C_{c2} in parallel and effectively added to C_{clk} and C_d . This would, in turn, reduce the necessary sizes of both L and C_d .

If both the parallel and series tank circuits are considered in Figure 1(a), the resonant frequency from Equation 3 is more accurately given as

$$f_{clk} = \frac{1}{2\pi} \sqrt{\frac{C_{clk} + C_d}{LC_{clk}C_d}}. \quad (5)$$

If $C_d = 10 \times C_{clk}$, this reduces to

$$f_{clk} = \sqrt{\frac{11}{10}} \frac{1}{2\pi\sqrt{LC_{clk}}}, \quad (6)$$

which shows a $\sqrt{11/10} = 4.9\%$ increase in resonant frequency due to the parasitic series LC_d tank. This can be utilized to reduce inductor size and save area at a fixed frequency.

If C_c is added in parallel with C_{clk} , the resonant frequency will add C_c to C_{clk} ,

$$f'_{clk} = \frac{1}{2\pi} \sqrt{\frac{C_{clk} + C_c + C_d}{L(C_{clk} + C_c)C_d}}. \quad (7)$$

If compared to Equation (5), this provides a

$$\frac{f'_{clk}}{f_{clk}} = \sqrt{\frac{1 + \frac{C_c}{C_{clk} + C_d}}{1 + \frac{C_c}{C_{clk}}}} \quad (8)$$

decrease in resonant frequency.

If we consider adding C_c in parallel with L , the resonant frequency will add C_{c1} to C_{clk} and C_{c2} to C_d ,

$$f'_{clk} = \frac{1}{2\pi} \sqrt{\frac{(C_{clk} + C_{c1}) + (C_d + C_{c2})}{L(C_{clk} + C_{c1})(C_d + C_{c2})}}, \quad (9)$$

where $C_{c1} = C_c(1 - A_v)$, $C_{c2} = C_c(1 - A_v^{-1})$, and A_v is the ratio of voltage after the L to before the L . Here, A_v is an approximation to calculate f'_{clk} . On the other hand, applying C_c directly to the formulation, the resonant frequency is

$$f'_{clk} = \frac{1}{2\pi} \sqrt{\frac{C_{clk} + C_d}{L[C_{clk}C_d + C_c(C_{clk} + C_d)]}}, \quad (10)$$

which gives a

$$\frac{f'_{clk}}{f_{clk}} = \sqrt{\frac{1}{1 + \frac{C_c}{C_{clk}} + \frac{C_c}{C_d}}} \quad (11)$$

decrease in resonant frequency. Since Equation (10) is strictly less than Equation (7), this provides more savings at all times.

A significant difference in the topologies is an additional capacitive effect (a_2) of C_{c2} to C_d when C_c is in parallel with L , where $a_2 = (f_d/f'_d)^2$. In this case, applying C_c to the formulation, the decoupling resonant frequency is

$$f'_d = \frac{1}{2\pi\sqrt{L(C_d + C_c)}}, \quad (12)$$

which is a factor $\frac{1}{\sqrt{C_c}}$ lower than the case without C_c . Consequently, it offers the advantage of sharing C_c directly from C_d for the same f_d .

Based on the resonant frequency in Equation (3), L can be reduced by adding C_c and considering the Miller approximation to get C_{c1} and C_{c2} . If $C_{c1} + C_{clk} = a_1 \cdot C_{clk}$, where a_1 is the ratio between capacitances, then L can be reduced as L/a_1 for the same resonant frequency (f_{clk}),

$$L' = \frac{L}{a_1} = \frac{L}{(f_{clk}/f'_{clk})^2}, \quad (13)$$

where $a_1 = (f_{clk}/f'_{clk})^2$ is the capacitive effect from C_{c1} , and L' and f'_{clk} are the inductance and resonant frequency after adding C_c , respectively.

Taking the derivative of Equation (13) for C_c in parallel with C_{clk} , we get

$$\frac{dL'}{dC_c} = L \frac{\frac{1}{C_{clk} + C_d} - \frac{1}{C_{clk}}}{(1 + \frac{C_c}{C_{clk}})^2}, \quad (14)$$

which is a negative slope with sharp or smooth L curve as C_c value decreases or increases. Doing the same derivative for C_c in parallel with L , we get

$$\frac{dL'}{dC_c} = L \frac{-\frac{1}{C_d} - \frac{1}{C_{clk}}}{(1 + \frac{C_c}{C_{clk}} + \frac{C_c}{C_d})^2}, \quad (15)$$

which is a negative, steeper slope for small C_c values. Therefore, C_c in parallel with L is a more effective topology in terms of reducing L .

IV. EXPERIMENTS

The experimental results are divided into two parts. All results are measured using HSPICE. The first part uses a buffered monolithic LC-tank to verify our theoretical analysis in Section III. The capacitance and inductance values are selected to represent a lumped CDN. The baseline resonant frequency (f_0) and V_{dd} are set to be 2GHz and 1V, respectively. The second part utilizes the concept of C_c insertion on a distributed resonant clock with the industrial-representative ISPD 2010 benchmarks from IBM and Intel [11]. The ISPD benchmarks are in a 45nm technology and use V_{dd} of 1V and f_0 of 1GHz. The resonant benchmark designs are synthesized using the Resonant Clock Synthesis (ROCKS) methodology [6] and the C++ source code is modified for our new circuit techniques.

A. Monolithic LC-tank

The first experiment verifies our previous theories using a monolithic LC-tank resonant clock with C_c insertion like Figure 2. A single LC tank loads a lumped clock grid ($C_{clk} = 5pF$), while $L = 1.39nH$ to achieve a desired resonant frequency of 2GHz. C_c was chosen to be $0.5C_{clk} = 2.5pF$ for demonstration, but as shown in Equation (14)-(15) the trends hold over all sizes.

The frequency analysis results are summarized in Table I. These verify that C_c in parallel with L enables a lower resonant frequency than in parallel with C_{clk} due to the higher capacitive effects (a_1 and a_2). Explicitly, f_{clk} with C_c in parallel with L shows 3.8% lower frequency than in parallel with C_{clk} , same as the theoretical models suggested in Section III. The parasitic decap resonant frequency (f_d) with C_c in parallel with L also matches the theoretical results in Equation (12).

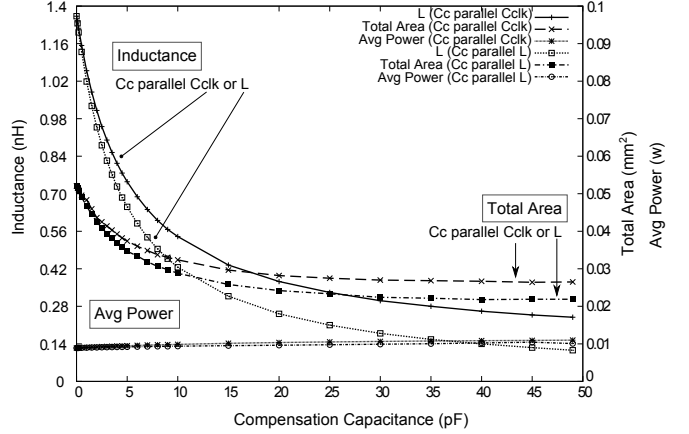


Fig. 3. For a 2GHz clock, C_c inserted in parallel with L saves more in terms of L and on-chip area, $\text{Area}(L) + \text{Area}(C_c) + \text{Area}(C_d)$.

Instead of changing resonant frequency, L and/or C_d can be reduced while maintaining the same frequency. For C_c in parallel with L , the capacitive effects are higher and C_d can be reduced in addition to L . Specifically, the capacitive effect (a_1) from C_{c1} suggests that L can be reduced as $L/a_1 = 1.39/1.55 = 0.90nH$ which also increases f_d . The trade-off between the L reduction and the range of resonant frequency separation (f_d vs f_{clk}) is based on Equation (3) resulting in a slightly tighter f_{clk}/f_d ratio. On the other hand, C_d could alternatively be reduced by 2.5pF which is equal to the inserted C_c and results in extra resource sharing. However, this is at the expense of higher f_d .

Finally, when we consider the actual on-chip inductor and capacitor areas as in Section II, Figure 3 shows the relationship between various C_c values and the total area ($\text{Area}(L) + \text{Area}(C_c) + \text{Area}(C_d)$) along with the power consumption. We assume that our inductor has $w = 15\mu m$, $s = 15\mu m$, and $d_i = 100\mu m$. We also assume a capacitive density of $10fF/\mu m^2$ for a typical MOS capacitor.

As seen in Figure 3, C_c insertion in parallel with L saves more in terms of L and on-chip area for all cases. The downside of this is that the power consumption goes up in both cases, but is explicitly lower when inserting C_c in parallel with L in all cases. This is because the voltage swing of the decap C_d is miniscule whereas C_{clk} has rail-to-rail swing. In our example $C_c = 2.5pF$, 21.4% total area is saved with only a 2.1% power increase and 10.4% inductor Q decrease when C_c is parallel with L . If we consider efficiency of saving area, the knee of the curve is at $C_c = 10pF$ which offers area savings of 44.7% with a power increase of 5.6% and inductor Q decrease of 29.5%.

B. Distributed LC-tanks

We then utilize C_c insertion in parallel with L in a distributed resonant clock synthesis (ROCKS) [6] methodology. ROCKS starts similar to Meshworks [12] by creating an initial buffered grid. ROCKS then places and sizes LC tanks to form a resonant grid using an iterative LC tank clustering algorithm. After this, ROCKS performs a frequency-based grid buffer

TABLE I. C_c INSERTION IN PARALLEL WITH THE INDUCTOR ENABLES A LOWER RESONANT FREQUENCY DUE TO THE HIGHER CAPACITIVE EFFECTS (a_1 AND a_2).

	f_{clk} (GHz)	Capacitive Effect (a_1)	L (nH) for same f_{clk}	L saving	f_d (mGHz)	Capacitive Effect (a_2)	C_d (pF) for same f_d	f_{clk}/f_d
C_c none	2.00	1	1.39	-	603.96	1	50	3.32
C_c parallel C_{clk}	1.67	1.43	0.97	30.17%	603.96	1	50	2.77
C_c parallel L	1.61	1.55	0.90	35.37%	589.11	1.05	47.5	2.67

$C_{clk} = 5\text{pF}$, $L = 1.39\text{nH}$, $C_d = 50\text{pF}$, and $C_c = 2.5\text{pF}$

TABLE II. C_c IMPLEMENTATION WITH DISTRIBUTED LC-TANKS ON ISPD 2010 BENCHMARKS SHOWS OVERHEAD REDUCTION AND MAINTAINS HIGH POWER SAVING.

Non-resonant CDN					ROCKS [6]				C_c implementation				
Sink #	Cap pF	Chip Area mm ²	Pwr ¹ mW	Pwr ² mW	Skew ps	LA/CA %	Pwr ² Saving %	Pwr ³ mW	Skew ps	LA/CA %	Q - %	Pwr ³ Saving %	
01	1107	18.9	64.0	327.2	203.7	41	29.2	37.7	204.2	41	17.1	18.6	37.6
02	2249	39.2	91.0	600.4	345.3	36	27.5	42.5	346.3	36	15.9	18.8	42.3
03	1200	18.1	1.4	114.7	32.6	33	30.7	71.6	47.0	42	19.3	20.4	59.0
04	1845	12.3	5.7	177.2	85.9	8	30.0	52.1	87.4	9	19.1	18.7	48.1
05	1016	5.2	5.8	111.4	40.3	9	29.6	60.5	52.9	13	17.8	19.1	52.5
06	981	12.6	1.5	103.0	27.4	25	36.2	73.4	39.7	30	21.9	19.0	61.5
07	1915	18.1	3.5	168.1	78.3	9	31.0	53.4	82.4	8	19.2	19.0	51.0
08	1134	13.0	2.6	117.7	49.0	13	28.2	58.3	59.6	12	17.7	23.2	49.4
Avg.	1431	17.2	21.9	213.8	107.7	22	30.3	56.2	114.9	24	18.5	19.6	49.9

Pwr¹: Switched capacitance CDN power. Pwr²: ROCKS power in HSPICE. Pwr³: C_c implementation power in HSPICE.
 LA/CA: Total inductor area normalized to metal layer (chip) area. Q - : Inductor Q decrease from L reduction in ASITIC [8].
 LA'/CA: Reduced total inductor area normalized to metal layer (chip) area.

sizing. Finally, a top-level buffered tree is generated with minimum wire length DME [13] to drive the resonant grid.

The C_c insertion is targeting the knee of curve in Figure 3 to save the most area. Table II organizes the power and inductor area analysis results and compared with a non-resonant grid, ROCKS, and our results with C_c insertion. For accurate comparison with ROCKS, the intrinsic resistances of inductor and capacitor are not taken into account since parasitic resistances of clock tree and grid dominate.

The inductor Q can be found by using $Q = \omega L/R_s$, where R_s is the parasitic resistance in series with L . R_s is obtained from ASITIC [8], assuming a single-layered square inductor model with no ground plane. A large Q can store more energy while a low Q does the opposite. Our results demonstrate that a distributed C_c -enhanced resonant clock reduces the inductor area overhead by approximately 11.8%, decreases the inductor Q about 19.6%, and still maintains nearly 49.9% power savings. This indicates that a C_c -enhanced LC circuit keeps the high amplitude at resonance, with a wider bandwidth around the resonant frequency.

V. CONCLUSIONS

Resonant clocks using distributed LC tanks hold great promise for power reduction by performing on-chip energy recycling in the form of the electrical and magnetic fields that resonate between the clock capacitance and an on-chip inductor. However, the size and area of inductance (L) and decoupling capacitance (C_d) are an extra cost that many designers wish to avoid. This paper demonstrated the concept of a compensation capacitor (C_c) to reduce this overhead in a resonant clock circuit. Our results show that L can be reduced most effectively by placing C_c in parallel with L rather than as additional clock capacitance load. This has the advantage of higher capacitive effects which result in both smaller L and C_d .

ACKNOWLEDGMENTS

This work was supported in part by the National Science Foundation under grant CCF-1053838.

REFERENCES

- [1] M. R. Guthaus, G. Wilke, and R. Reis, "Revisiting automated physical synthesis of high-performance clock networks," *TODAES*, vol. 18, no. 2, pp. 31:1–31:27, Apr. 2013.
- [2] S. C. Chan, K. L. Shepard, and P. J. Restle, "Design of resonant global clock distributions," in *ICCD*, 2003.
- [3] F. O'Mahony, C. Yue, M. Horowitz, and S. Wong, "Design of a 10GHz clock distribution network using coupled standing-wave oscillators," in *DAC*, 2003, pp. 682–687.
- [4] V. Chi, "Salphasic distribution of clock signals for synchronous systems," *IEEE Trans. on Comp.*, vol. 43, no. 5, pp. 597–602, 1994.
- [5] J. Rosenfeld and E. G. Friedman, "Design methodology for global resonant H-tree clock distribution networks," *IEEE TVLSI*, vol. 15, no. 2, Feb 2007.
- [6] X. Hu and M. Guthaus, "Distributed LC resonant clock grid synthesis," *TCAS-I*, vol. 1, 2012.
- [7] Y.-S. Choi and J.-B. Yoon, "Experimental analysis of the effect of metal thickness on the quality factor in integrated spiral inductors for RF ICs," *IEEE Electron Device Lett.*, vol. 25, no. 2, pp. 76–79, Feb 2004.
- [8] A. M. Niknejad, S. Member, and R. G. Meyer, "Analysis, design, and optimization of spiral inductors and transformers for Si RF IC's," *JSSC*, vol. 33, pp. 1470–1481, 1998.
- [9] M. Popovich, A. V. Mezhiba, and E. G. Friedman, *Power Distribution Network with On-Chip Decoupling Capacitors*. Springer, 2007, ch. 6.
- [10] B. Razavi, *Design of Analog CMOS Integrated Circuits*. McGraw-Hill, 2001, ch. 6.
- [11] C. N. Sze, "ISPD 2010 high performance clock network synthesis contest," in *ISPD*, 2010.
- [12] A. Rajaram and D. Z. Pan, "Meshworks: an efficient framework for planning, synthesis and optimization of clock mesh networks," in *ASP-DAC*, 2008.
- [13] T.-H. Chao, Y.-C. Hsu, and J. Ho, "Zero skew clock net routing," in *DAC*, 1992, pp. 518–523.